AD-A087 682 UNITED TECHNOLOGIES RESEARCH CENTER EAST HARTFORD CONN F/G 20/5
INVESTIGATION OF DISCHARGE PROCESSES IN ELECTRICALLY EXCITED BL--ETC(U)
JUL 80 W J WIEGAND N00014-79-C-0593
UNCLASSIFIED UTRC-R80-924780-1 NL

1 OF 1
AD
A087682

END
DATE
FILMED
9-80
DTIC

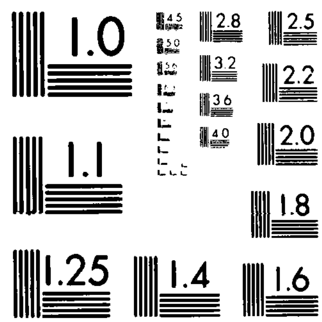

MICROCOPY RESOLUTION TEST CHART
NATIONAL BUREAU OF STANDARDS-1963-A

R80-924780-1

LEVEL II

12

INVESTIGATION OF DISCHARGE PROCESSES IN ELECTRICALLY EXCITED BLUE/GREEN LASERS

Prepared By
W.J. Wiegand

Final Report
July 31, 1980

Sponsored by the Naval Ocean Systems Center
Under Contract N00014-79-C-0593

UNITED TECHNOLOGIES RESEARCH CENTER
EAST HARTFORD, CONNECTICUT 06108

(14) UTRC - R80-924780-1

(6) Investigation of Discharge Processes in Electrically Excited Blue/Green Lasers.

(10) Walter J. Wiegand

(9) Final Rep[redacted]t. 1 Jun 79-31 May 8[illegible]

(11) 31 Jul[redacted]980

(12) 47

Sponsored by the Naval Ocean Systems Center
Under Contract N00014-79-C-0593 (15)

United Technologies Research Center
East Hartford, Connecticut 06108

401252

UNCLASSIFIED

SECURITY CLASSIFICATION OF THIS PAGE (When Data Entered)

REPORT DOCUMENTATION PAGE		READ INSTRUCTIONS BEFORE COMPLETING FORM
1. REPORT NUMBER R80-924780-1	2. GOVT ACCESSION NO. AD-A087 682	3. RECIPIENT'S CATALOG NUMBER
4. TITLE (and Subtitle) INVESTIGATION OF DISCHARGE PROCESSES IN ELECTRICALLY EXCITED BLUE/GREEN LASERS		5. TYPE OF REPORT & PERIOD COVERED Final Report June 1, 1979 to May 31, 1980 6. PERFORMING ORG. REPORT NUMBER R80-924780-1
7. AUTHOR(s) Walter J. Wiegand		8. CONTRACT OR GRANT NUMBER(s) N00014-79-C-0593
9. PERFORMING ORGANIZATION NAME AND ADDRESS United Technologies Research Center Silver Lane East Hartford, CT 06108		10. PROGRAM ELEMENT, PROJECT, TASK AREA & WORK UNIT NUMBERS
11. CONTROLLING OFFICE NAME AND ADDRESS Office of Naval Research Physics Program Office 800 No. Quincy St., Arlington, VA 22217		12. REPORT DATE July 1980 13. NUMBER OF PAGES 47
14. MONITORING AGENCY NAME & ADDRESS(if different from Controlling Office)		15. SECURITY CLASS. (of this report) Unclassified 15a. DECLASSIFICATION/DOWNGRADING SCHEDULE

16. DISTRIBUTION STATEMENT (of this Report)

Approved for public release; distribution unlimited.
Reproduction in whole or in part is permitted
for any purpose of the United States Government.

17. DISTRIBUTION STATEMENT (of the abstract entered in Block 20, if different from Report)

18. SUPPLEMENTARY NOTES

The principal findings of this investigation have been submitted for publication in Applied Physics Letters.

19. KEY WORDS (Continue on reverse side if necessary and identify by block number)

Ionization of $HgBr_2$, Electron Attachment in Mercuric Bromide, Dissociative Attachment in $HgBr_2$, Electron Production and Loss Processes in $HgBr_2$ Lasers, Discharge Processes in $HgBr_2$ Lasers, Mercuric Bromide Dissociation Lasers.

20. ABSTRACT (Continue on reverse side if necessary and identify by block number)

Total and partial cross sections for mercuric bromide ($HgBr_2$) electron attachment and ionization reactions of importance in laser discharges have been measured in electron beam experiments. Corresponding rate coefficients have been determined independently in a pulsed, electron swarm apparatus. These studies have determined that the electron impact ionization cross section of $HgBr_2$ is very large, increasing from a threshold at 10.6 eV to a

(Continued)

DD FORM 1 JAN 73 1473 EDITION OF 1 NOV 65 IS OBSOLETE

S/N 0102-LF-014-6601

UNCLASSIFIED

SECURITY CLASSIFICATION OF THIS PAGE (When Data Entered)

10 to the minus 15th power

Abstract (Continued)

sq cm

ion

10 to the minus 17th power

value of 2×10^{-15} cm^2 at 70 eV, with $HgBr_2^+$ being the principal ion formed at low energies. Beam measurements also have revealed only one electron loss process, dissociative attachment. This attachment reaction which produces Br^- has a threshold energy of 3.1 eV and a peak cross section of 1×10^{-17} cm^2 at 3.7 eV. From swarm measurements, an attachment rate coefficient of 1.5 x 10^{-10} cm^3 sec^{-1} at a few electron volts average electron energy has been determined. This value is consistent with cross section values determined from beam measurements and with values inferred from kinetic modeling studies of electron beam controlled $HgBr_2$ laser discharges.

ion

sq cm

10 to the minus 10th power cu cm/sec

S/N 0102-LF-014-6601

PREFACE

Under the present Contract, United Technologies Research Center has conducted a basic experimental and analytical investigation of electron production and loss processes in mercuric bromide ($HgBr_2$). Total ionization and attachment cross sections have been measured and product ions have been identified. Attachment and ionization rate coefficients have been determined independently. This work was carried out in close coordination with other Corporate- and Navy-sponsored experimental and theoretical programs.

Technical support in this program was provided by L. R. Boedeker who was responsible for the electron swarm measurements, by W. L. Nighan who furnished the Boltzmann code computations and guidance on gas mixtures for the swarm experiments and by A. C. Eckbreth and C. M. Ferrar who provided assistance in photosource development. Their many contributions are gratefully acknowledged. The enthusiastic support and encouragement of these investigations by R. H. Bullis is greatly appreciated.

R80-924780-1

Investigation of Discharge Processes in Electrically Excited Blue/Green Lasers

TABLE OF CONTENTS

I. INTRODUCTION

A. Background

The mercuric bromide dissociation laser is a leading candidate for Navy applications requiring high efficiency at blue/green wavelengths. Progress has been made at a rapid pace in the development of both fast-pulse[1] and electron beam sustained[2] discharge excitation of this laser. During the past several years, understanding of the specific mechanisms which lead to efficient HgBr(B) formation in the $HgBr_2$ dissociation laser has increased significantly. Rate coefficients for $HgBr_2$ excitation transfer[3,4] from a number of electronically excited species which can give rise to the $HgBr^*$ (B→X) transition at wavelengths near 502 nm are now available. However, until recently, the modeling of this laser system has been hampered by a lack of data on the rates of formation of positive and negative ions created by electron impact on $HgBr_2$. The basic experimental and analytical research program reported herein was directed toward determination of both the ionization and attachment rate coefficients for $HgBr_2$ in the electron energy range typical of laser operation.

Specific accomplishments under this Contract included the measurement of both the mercuric bromide ($HgBr_2$) electron attachment and ionization cross sections and the rate coefficients for these processes using independent experimental approaches. The energy range of these measurements extended beyond the conditions of interest to $HgBr_2$ laser operation. In addition, the product ions resulting from these reactions were mass identified. As a further independent check, the results of these measurements were compared with values or the electron attachment rate derived from modeling studies of electron beam controlled $HgBr_2$ laser discharges conducted under a separate Navy contract[5].

B. Principal Program Results

The principal results of this investigation can be summarized as follows:

- The total cross section for electron attachment in $HgBr_2$ has been determined by beam measurements to have a threshold of 3.1 eV with a peak cross section value of 1.0×10^{-17} cm^2 occurring at 3.7 eV. Mass spectrometric analysis reveals that negative ion formation is limited to this single dissociative attachment process which forms Br^- at low electron energies. The measured 3.1 eV threshold for Br^- formation suggests that the upper laser level, $HgBr(B^2\Sigma^+)$, is the other reaction product as has been proposed recently by Degani, Rokni and Yatsiv[6].
- The dissociative electron attachment rate coefficient has been determined from completely independently pulsed electron swarm measurements to have a value of 1.5×10^{-10} cm^3-sec^{-1} for electric field to neutral gas density ratios (E/N's) corresponding to average electron energies typical of those encountered in mercuric bromide laser discharges. This measured value is consistent with the above reported beam measurements and recent values of attachment rates determined from flash X-ray ionization experiments[6]. It should be noted, however, that the preliminary attachment rate coefficient determined by Nygaard and coworkers[7] is not in agreement with the comparatively low rate coefficient for attachment determined in these independent experiments. The discrepancy between the two sets of results was resolved experimentally in this investigation and is discussed in Section III of this report.
- The total electron impact ionization cross section of $HgBr_2$ has been found from beam measurements to have a threshold of 10.6 eV with a value of 2.0×10^{-15} cm^2 at the calibration energy of 70 eV. These measurements are the first to establish the absolute magnitude of the $HgBr_2$ ionization cross section. The principal ion produced near threshold energies was found to be $HgBr_2^+$. In addition, partial cross sections for the formation of $HgBr_2^+$ and

the several minor fragment ions ($HgBr^+$, Br^+, Hg^+) have been inferred from mass spectrometer measurements.

- Complementary electron swarm measurements have provided ionization rate coefficients in agreement with those computed from the electron beam-measured ionization cross sections.
- Verification of the results of this program has been obtained from the inferred values of the ionization and attachment rate coefficients derived from the kinetic modeling of electron beam controlled $HgBr_2$ laser discharge characteristics obtained by Brown and Nighan under a separately sponsored UTRC-Navy program[5].

II. ELECTRON BEAM MEASUREMENTS

A. Technique

A singularly successful technique for measuring electron impact ionization and attachment cross sections is the beam method developed nearly forty years ago by Tate and Smith[8]. Until recently this original work stood as the standard data on ionization in simple gases. Refinements of the Tate and Smith method have since provided the widely used data of Rapp and coworkers[9-11] on atmospheric and rare gases, while the work of Chantry[12] and Kurepa, et al.[13,14] has provided data on several electronegative gases.

The Tate-Smith method consists of firing a magnetically collimated electron beam through a nearly field-free collisional chamber containing the subject gas at a known concentration. The gas density is set such that minimal attenuation of the electron beam occurs. Positive or negative ions formed as a result of ionizing or attaching collisions are only weakly influenced by the applied magnetic field and are collected under the influence of a low intensity, transverse electric field applied to electrodes located at opposite sides of the collision chamber. Due to the collimating magnetic field scattered electrons cannot reach these collectors. The remaining primary electron beam current is measured on a collector located beyond the far end of the chamber. The cross section, Q, for the process of interest, is then ccmputed from the measured ion current, I_I, the electron current, I_e, the gas concentration N, and the beam path, L, using the simple expression:

$$Q = I_I/I_e NL \quad . \tag{1}$$

Additional detailed information regarding the ion formation processes is obtained by mass analysis of product ions which can be sampled through an aperture in the collision chamber sidewall.

B. Apparatus

The UTRC beam experiment used in this study was of the Tate-Smith configuration with ion analysis provided by a quadrupole mass spectrometer. Data acquisition and control of experimental parameters was automated through the use of a dedicated DEC 1140 computer which also provided signal processing capabilities.

The collision chamber and mass spectrometer were housed in a stainless steel vacuum chamber whose 10^{-7} torr base pressure was maintained by a LN_2 trapped diffusion pump. All portions of the vacuum system surrounding the collision chamber and mass spectrometer were superheated to 390°K to avoid the possibility of forming a secondary $HgBr_2$ reservoir. The mercuric bromide powder was introduced into the system through a temporary glass appendage which permitted vacuum distillation of the $HgBr_2$ directly into the primary reservoir. During calibration, krypton and xenon were leaked from an external manifold into the collision chamber through the reservoir. For reasons of possible materials incompatibility, the Granville-Phillips variable leak valve used for this purpose was protected from direct contact with the bromide vapor by a normally closed, all stainless steel valve. A 19 mm glass tube which constituted the $HgBr_2$ reservoir extended from below the main vacuum system into one side of the collision chamber. A temperature stabilized warm water bath immersing the lower portion of the reservoir tube was utilized to control the $HgBr_2$ vapor pressure during data acquisition. Reservoir pressure was set based on the measured bath temperature and published vapor pressure data[15]. However, as elaborated below, the pressure used in determination of the gas concentration in the collision chamber was obtained from the readings of an MKS Baratron capacitive pressure transducer located at a point midway between the reservoir and the interior of the collision chamber. The Baratron was separated from continuous contact with the reservoir by an all stainless steel valve; however, exposure to $HgBr_2$ could not be avoided during pressure determinations. With the exception of small portions of this pressure transducer, there was no contact of the $HgBr_2$ with materials other than glass, 300-series stainless steel or high density alumina until the vapor was lost through collision chamber apertures to the low pressure region of the vacuum system.

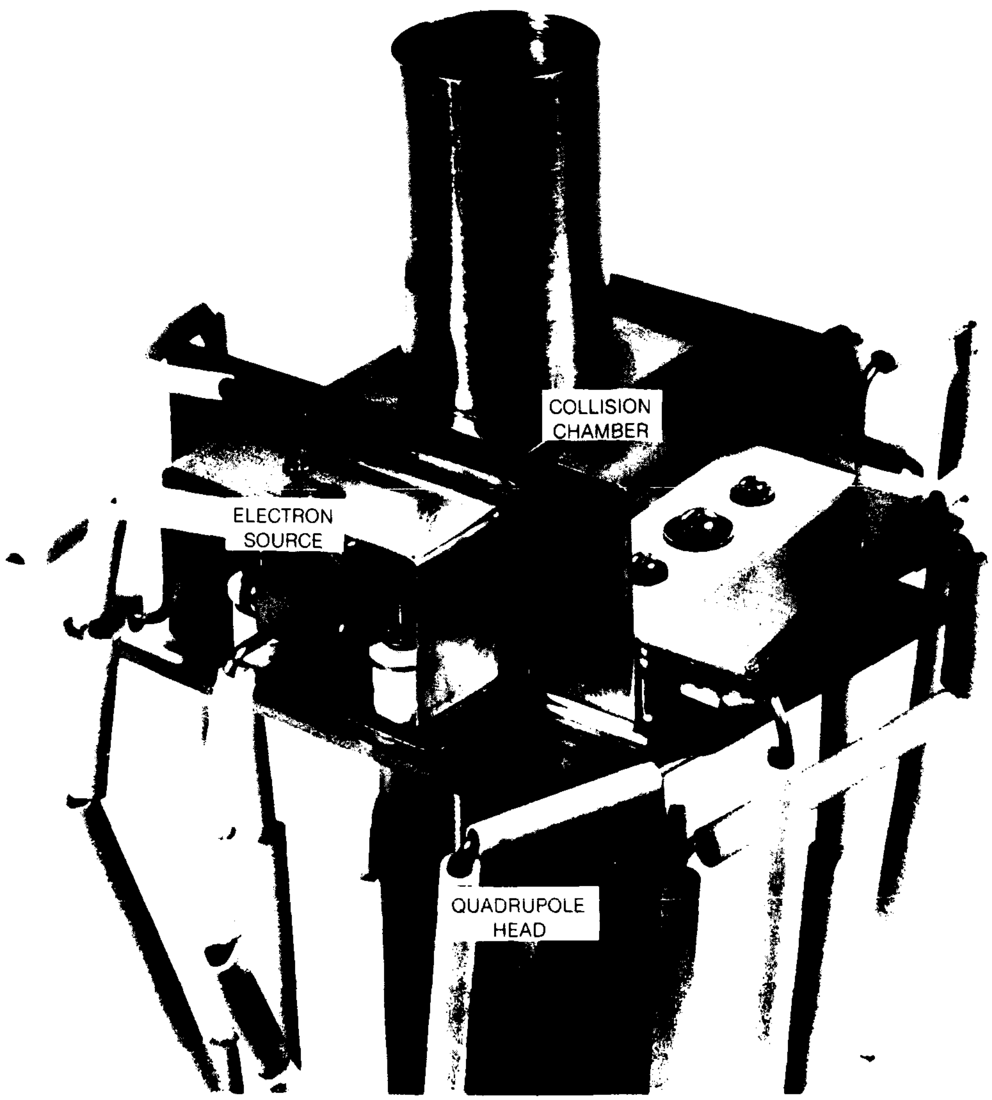

Figure 1. The collision chamber assembly as mounted on the quadrupole head. This view is from the electron source end. The sleeve at the top mates to the glass reservoir tube. The orientation of this unit in the beam apparatus is inverted from that shown in the figure.

80-126-B

80-7-94-9

Two collision chamber assemblies were used in the course of these investigations. Each was mounted directly at the entrance end of the quadrupole mass spectrometer head in place of the commercial ionizer section. The simpler initial structure was used to verify the compatibility of the thoriated iridium filament and the Channeltron ion multiplier with the mercuric bromide vapor. In addition, the general chamber design and materials suitability, the methods of $HgBr_2$ handling, the refinements in the computer control and the magnetic field intensity requirements were evaluated with the first chamber. A preliminary estimate of the ionization cross section and a survey of the ion species formed in electron collisions also were made with this initial assembly. Based on the generally favorable results obtained from the initial measurements, a second slightly modified chamber was constructed.

This collision chamber incorporated two refinements of the original design: an increase in collision chamber length to 3.34 cm and the addition of guard electrodes surrounding the ion attractor. The general features of this collision chamber design can be seen in Fig. 1, which is a view of the assembly as mounted on the quadrupole head. The principal features of the chamber are more readily described by reference to the schematic of the apparatus presented in Fig. 2a and the corresponding potential profile in Fig. 2b. Briefly, the beam is established by the source, which consists of the dc heated filament, FILA, the electron extracting electrode, EXTR, and the retarding potential difference plate, RPD. The EXTR and RPD potentials are referenced with respect to the center potential of the filament, which is swept negatively relative to the collision chamber, CHAMB, to provide a beam of increasingly energetic electrons in the collision region. Depending on the potential of the RPD plate relative to the filament voltage, the beam source can be operated in a steady-state RPD mode or as a conventional electron source. In the RPD mode[16,17], the voltage increment is provided on alternate electron energy sweeps. The RPD method was only used in the high energy resolution measurements due to the significant loss of signal incurred in this mode of operation. Operationally, the lower and upper voltage limits of the beam energy and the number of sweeps were keyboard programmable through a dedicated PDP 11 computer, whereas the rate and magnitude of the voltage ramp for

a.

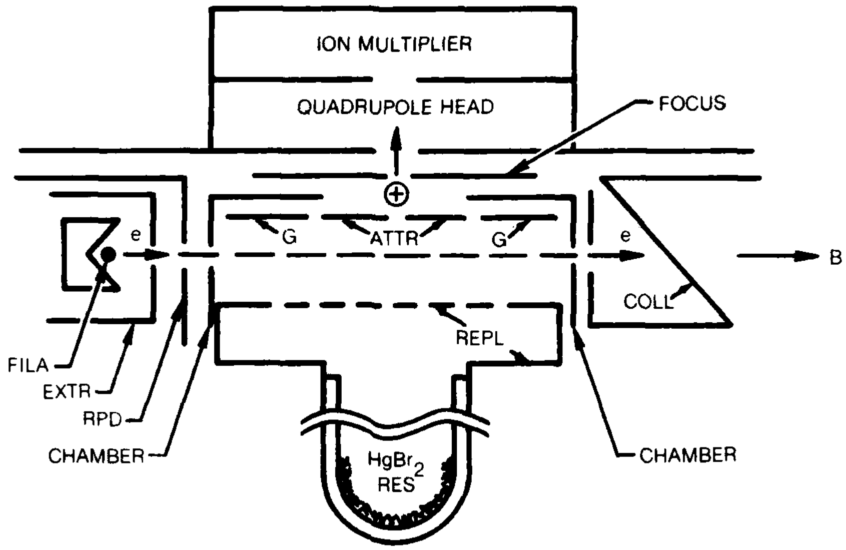

b.

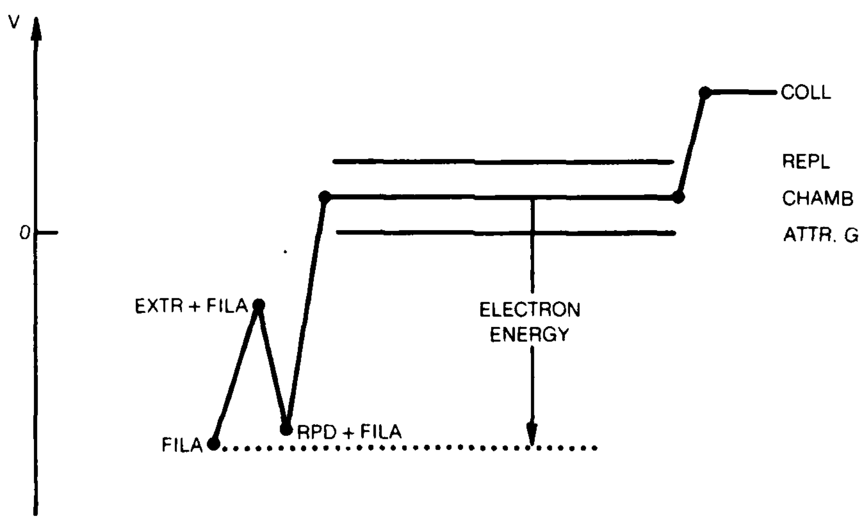

Figure 2. Schematic of the collision chamber (a) with a typical voltage profile along the electron beam path (b). The profile (b) is representative of a positive ion tune. For negative ion observation, the polarities of REPL and CHAMB must be reversed.

80-7-94-1

beam energy control and correlated storage of measured current/count data were functions of a Tracor Northen NS-570A multichannel analyzer coupled to the computer system.

The electron beam was constrained to a nearly linear path in the collision chamber by a field of up to 600 Gauss which was provided by external electromagnets. The collision chamber proper was comprised of four elements: the end faces of the chamber, CHAMB, which contained the beam entrance and exit apertures; the repeller, REPL, which consisted of a perforated sidewall backed by a small plenum with a sleeve for coupling to the reservoir tube; the attractor, ATTR, with its aperture to permit passage of ion samples to the spectrometer; and guard electrodes, G, which minimized leakage currents to the attractor and defined its ion collection length. The chamber elements were formed from 0.25 mm stainless steel stock, insulated from each other by alumina spacers, and when assembled into the collision chamber constituted a nearly vapor-tight enclosure. Finally, the collector electrode, COLL, was configured such that beam electrons first passed through an aperture near the chamber exit before impinging on its canted face. This collector design, in the presence of the B-field, minimized the possibility of reflected or secondary electrons returning to the collision chamber.

Tune of the collision chamber electrodes is determined by several considerations: the need to sustain the potential on the electron beam path equal to chamber potential, the requirement for a sufficient transverse field between the repeller and attractor/guard electrodes to saturate ion current collection and the polarity of the ions being measured. To permit observation of the ions by the quadrupole spectrometer, whose entrance aperture was grounded, the chamber voltage was typically several volts positive in ionization studies and a like amount negative for the attachment measurements. For experimental convenience, the attractor and its guard operated at ground potential, the former being connected to the input of a Keithley electrometer. Thus, the repeller operated a nominal several volts above chamber potential with the exact setting being determined such that beam cut off at zero energy occurred at or just inside the chamber entrance. The collector current was measured with a second Keithley electrometer in series with a +22 V bias battery.

Selectively, the output signals from either of the electrometers could be sent to the multichannel analyzer for subsequent evaluation of the cross sections.

The ion species produced in electron-$HgBr_2$ collisions were determined by extracting a portion of the attractor-directed ion current through an aperture in that electrode, providing some acceleration with the focus plate, FOCUS (Fig. 2), and observing the mass spectra. An Electronic Associates Quad 200 Residual Gas Analyzer utilized for this purpose was equipped with a Channeltron 4039 (Ruggedized) ion multiplier which was used in the pulse counting mode. Since multiplier gain deteriorated during measurements of $HgBr_2$ fragment ions, observation at the lowest feasible chamber pressure and sampling current level was required. The electron energy correlated counts were accumulated for the selected number of sweeps in the Tracor multichannel analyzer which served as a buffer memory. The data subsequently was transferred to the DEC PDP 11 computer for processing.

C. Calibrations

Absolute energy scales and magnitudes for the cross sections of $HgBr_2$ were established by calibrations with krypton and xenon, whose ionization cross sections are well-known[9]. At the submillitorr pressures of these studies, pressure relationships and gas transport properties are characterized by free molecular flow considerations[9]. Thus, while the loss rate of gas from the chamber to the surrounding vacuum is mass dependent, the relationship of the pressure as measured by the Baratron gauge to that in the collision chamber remains species independent[9]. Calibration gas was leaked into the chamber to various pressures in the 10^{-3} torr range. The electron energy dependence of the measured attractor-to-beam current ratio, I_I/I_e, which is proportional to the ionization cross section was found to be in very good agreement with that measured by Rapp and Englander-Golden[9]. Using the magnitudes of Q_i at 70 eV as determined by these investigators for Kr and Xe, the gas density in the collision chamber, N, was computed from Eq. 1. Comparison of this value with that determined upstream from temperature corrected capacitance manometer readings established the calibration factor for the Baratron measurements. This factor of 0.33 $\pm$ 10 percent was found to be independent of chamber tune, beam current

level, magnetic field intensity above 200 Gauss, gas pressure and calibrating gas as required for this method to be a proper calibration procedure. Using this calibration factor, $HgBr_2$ concentrations in the collision chamber were determined from the capacitance manometer readings during mercuric bromide cross section measurements.

The linear voltage sweep of the electron beam was calibrated to an absolute energy scale using current cut off at zero energy and the well established[18] thresholds for ionization of Xe (12.1 eV) and Kr (14.0 eV) for reference voltages.

D. Experimental $HgBr_2$ Ionization Cross Sections

The total electron impact cross section for ionization of mercuric bromide was determined from threshold to 70 eV using the methods outlined above. Additionally, the yield of $HgBr_2^+$ and the several fragment ions was observed mass spectrometrically over the same energy range.

The total ionization cross section of $HgBr_2$ was determined from measurements of beam current, I_e, attractor current, I_I, gas concentration, N, and attractor electrode length, L = 1.10 cm, using Eq. 1. Electron beam currents in the 10^{-8} A to low 10^{-7} A range were selected in order to eliminate space change effects of the source. Ion currents to the attractor were limited to several percent of this beam current by selecting reservoir temperatures corresponding to vapor densities of $HgBr_2$ in the collision chamber of 10^{12} cm^{-3} to 10^{13} cm^{-3}. Over these ranges of parameters and for all magnetic fields above 200 Gauss and reasonable variations in the chamber tune, a common cross section was determined.

The measured total cross section for ionization of $HgBr_2$ by electrons is shown in Fig. 3. As is typical of many gases, the total ionization cross section is a generally featureless function of electron energy rising nearly linearly at first from threshold (10.6 eV for $HgBr_2$) toward a maximum above 70 eV. The magnitude of the total cross section at the 70 eV calibration energy is 2×10^{-15} cm^2 with an estimated error of $\pm$ 25 percent due mostly to gas density uncertainty.

The simple appearance of the total ionization cross section tends to mask the fact that it is a charge weighted summation of a half-dozen partial cross sections

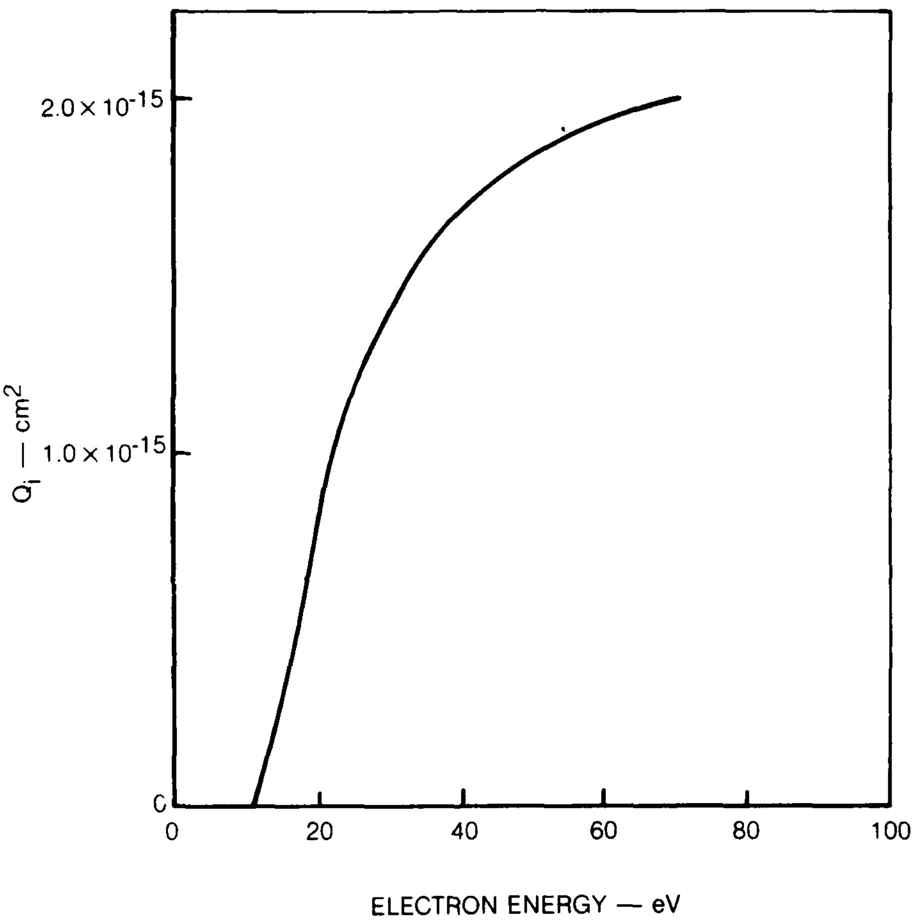

Figure 3. Measured total ionization cross section of mercuric bromide, $HgBr_2$.

80-7-94-2

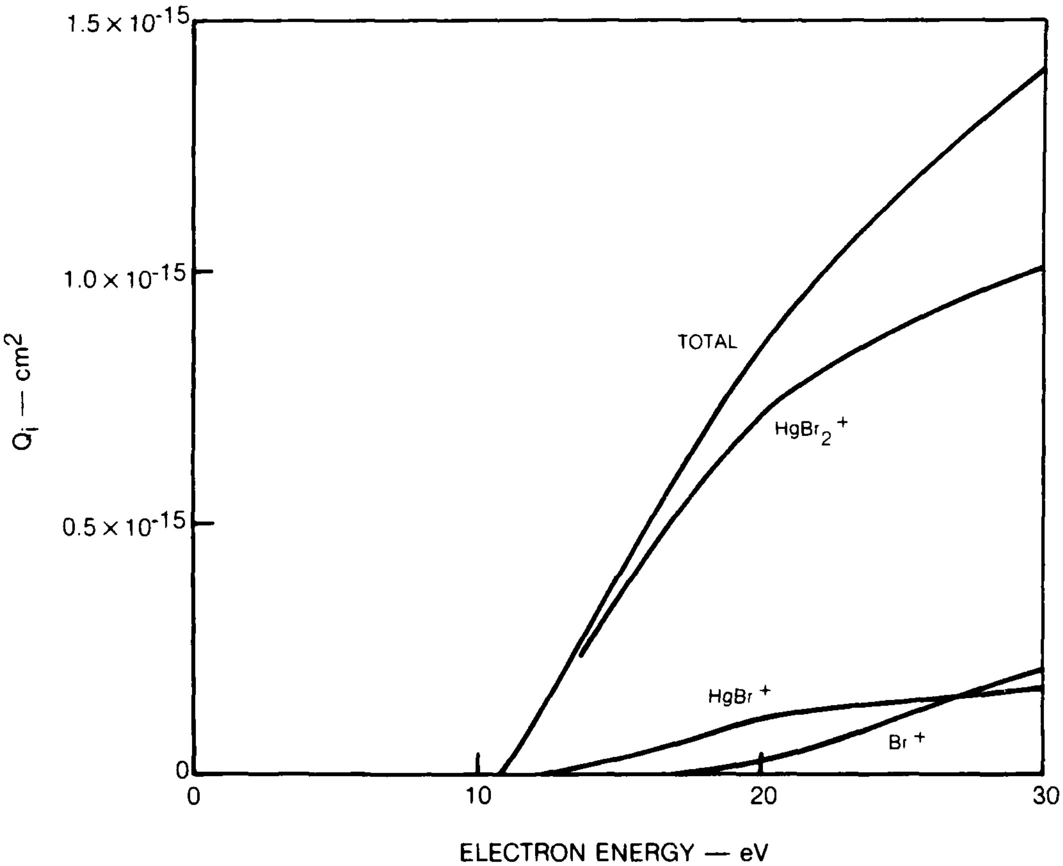

Figure 4. Partial cross sections of $HgBr_2^+$ and fragment ions compared with the total cross section.

each having its own threshold and energy dependence. From mass spectrometer measurements information regarding these partial cross sections was derived. Ionization processes leading to the production of the singly charged ions $HgBr_2^+$, $HgBr^+$, Br^+ and Hg^+ contribute to the total ionization level at low energies whereas $HgBr_2^{++}$, $HgBr^{++}$ and Br^{++} formation contribute to the net electron yield at high energies. Placing the partial cross sections on a true relative scale is not possible in the beam experiment due to the unknown transmission efficiency of the ion extraction optics and the quadrupole mass spectrometer over such a broad ion mass range. Fortunately, relative abundances of $HgBr_2^+$, $HgBr^+$, Br^+ and Hg^+ produced from mercuric bromide have been measured[19,20] at 70 eV in a time-of-flight instrument wherein the response is relatively independent of ion mass. Using these published results to normalize the partial cross sections[21], the relative production of the several ions can be estimated as shown on Fig. 4. An absolute calibration of the magnitude of these cross sections is determined by setting their sum equal to the measured total cross section at 30 eV. The lower ionization threshold and greater magnitude of the cross section for $HgBr_2^+$ formation indicated in Fig. 4 clearly implies that production of this ion will be strongly favored under fast pulsed laser discharge conditions.

Additional measurements of $HgBr_2$ ionization are discussed in connection with the pulsed electron swarm experiment in Section II and further implications of these results to the mercuric bromide laser will be elaborated upon in Section IV.

E. $HgBr_2$ Dissociative Attachment

Operation of the beam experiment with key potentials reversed provided information on negative ion processes. The total electron attachment cross section in $HgBr_2$ was found to consist of a single peak located between 3.1 eV and 4.5 eV. Mass spectrometer analysis revealed that the process being observed was dissociative attachment leading to Br^- formation. The measured electron energy dependence of the attachment cross section is shown in Fig. 5. Its peak value of 1×10^{-17} cm^2 at 3.7 eV was determined in alternate calibrations of the peak attachment cross section, and the total ionization cross section at 70 eV. These joint calibrations were obtained at common $HgBr_2$ reservoir temperatures over a range in $HgBr_2$ densities

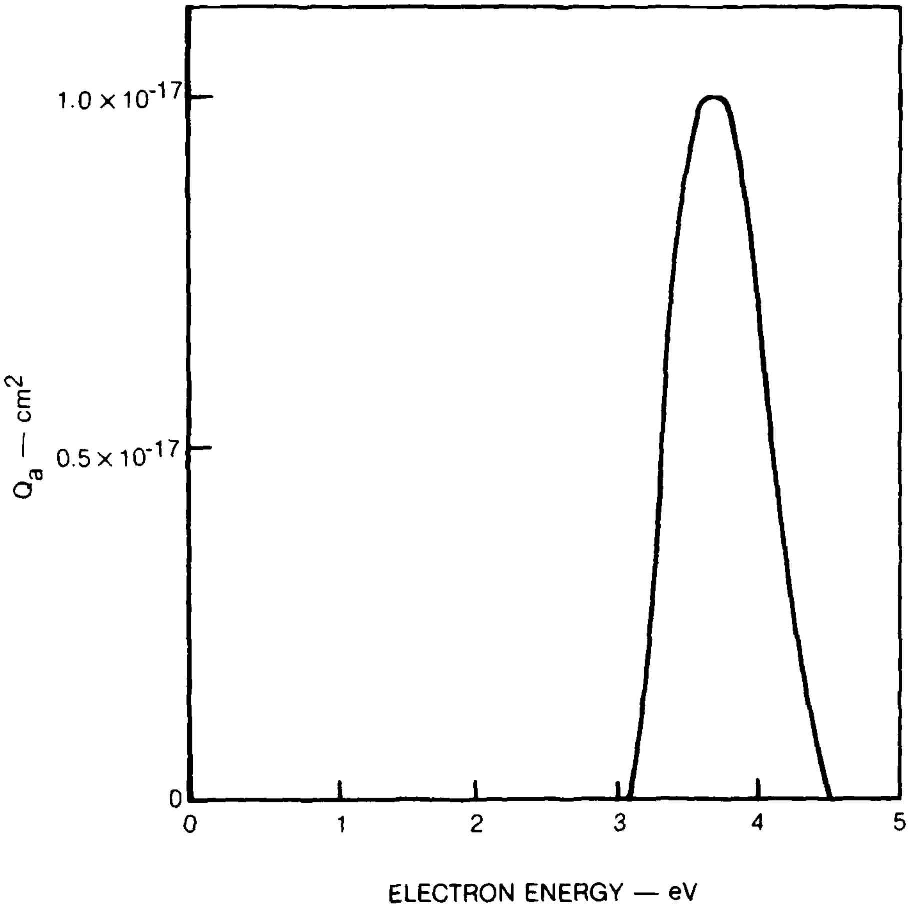

Figure 5. Measured electron attachment cross section of mercuric bromide, $HgBr_2$. The process is dissociative attachment forming Br^-.

80-7-94-4

varying by a factor of ten and centered at a vapor concentration of 3×10^{12} cm^{-3}. Owing to uncertainties in the mercuric bromide chamber density, N, and the less than 10^{-11} A I_I current levels of these attachment measurements, the uncertainty of the peak attachment cross section is estimated to be $\pm$ 30 percent. The value of Q_i(70 eV)/Q_a(3.7 eV) of 190, which was determined from these joint calibrations, is undoubtedly more accurate than the individual magnitudes due to cancellation of the gas density terms in the ratio. Additional information regarding the magnitude of the attachment cross section was derived independently from the swarm measurements which will be discussed in the next section.

III. ELECTRON SWARM MEASUREMENTS

A. Technique

An electron swarm experiment can provide a direct measure of the rate coefficient, k, for production or loss of electrons due to ionization or attachment reactions. This independent technique is complementary to the beam studies and is especially useful when the cross section for the process is narrow in energy and/or exists only near zero energy as is frequently the case for attachment. In these circumstances the measurement of the velocity weighted cross section average as determined in the electron swarm technique can provide a more accurate magnitude for the process than can the beam measurements which may suffer from resolution problems under these conditions.

The pulsed swarm technique used in these studies is based on the integral method pioneered by Grünberg[24]. In this approach a narrow burst of electrons is photoemitted into a constant field region between two parallel electrodes by a flash of light from a suitable source. When a proper mixture of the attaching gas and a buffer is present in the interelectrode gap, attachment processes convert a portion of the rapidly drifting electron group into less mobile negative ions. The integral of the current induced in the external circuit by the motion of these electrons and negative ions has a distinctive waveform which is readily interpreted in terms of the attachment rate. This method with refinements has been used in the study of attachment reactions in a number of halogen bearing molecules recently[7,23]. A review[23] of this work by Nygaard, Brooks, and Hunter describes a typical apparatus, details the analysis of experimental waveforms, and provides data on attachment in a number of gases.

B. Apparatus

<u>Cell</u>

A partial schematic of the UTRC swarm experiment is indicated in Fig. 6. A glass cell was provided with a quartz window and a set of identical planar electrodes.

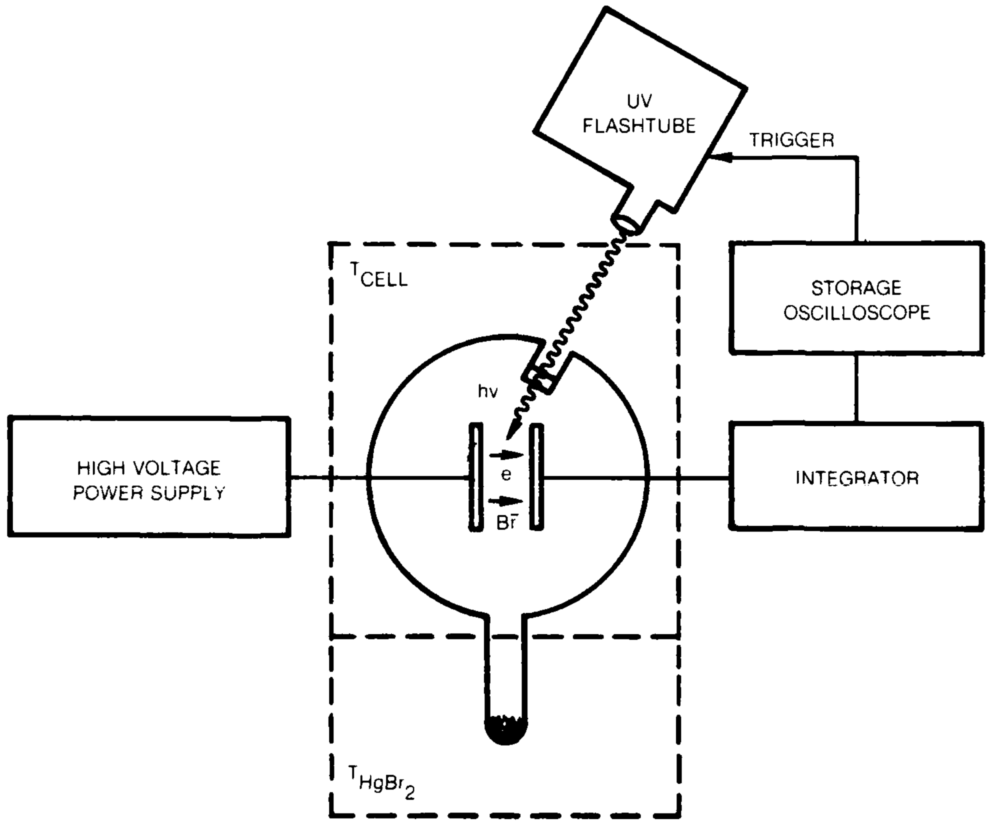

Figure 6. Schematic of the pulsed, electron swarm experiment. The cell region is superheated such that the mercuric bromide vapor density will be controlled by the reservoir temperature.

80-7-94-5

This cell was isolated from the gas manifold and the vacuum station by high vacuum valves. To minimize reactions with $HgBr_2$, all electrodes, vacuum feedthroughs and valve surfaces exposed to the cell interior were stainless steel. Additionally, the cell design incorporated a vertical tabulation which served as the $HgBr_2$ reservoir and a temporary appendage which was utilized in loading and vacuum distilling the mercuric bromide powder into the reservoir. System pressure, as indicated by external ionization gauges, could be maintained in 10^{-6} torr range with the bromide held at ice temperature. Increased pumping speed for initial outgassing of the $HgBr_2$ was provided by a LN_2 trap adjacent to the vacuum station valve.

In addition to providing access to the gas supplies, the normally closed manifold valve protected the Baratron pressure transducer used in establishing the buffer gas pressure from exposure to the $HgBr_2$ vapor. The mercuric bromide concentration in these measurements was determined from its vapor pressure[15] at the reservoir temperature corrected for the superheat temperature of the upper cell. During data acquisition, the reservoir temperature was maintained by a well-stirred hot oil bath and was measured directly with thermocouples. The cell itself was superheated by an integral oven consisting of multiple layers of aluminum foil wrapped directly on the glass, then overwrapped with heater tapes and finally with a heavy layer of thermal insulation. This construction equalized cell heating but more importantly, the presence of the foil layer provided an electrical noise shield and a low inductance continuation of the ground path between the emitting electrode voltage supply and the sensitive integration circuits attached to the collecting electrode. Thermocouples at three locations on the cell wall indicated a superheat temperature uniformity of better than 5°K at 420°K.

Integrators

The electrodes of this cell were 2.5 cm in diameter and were fixed at a separation of 9.7 mm. Connected to the emitting electrode was a well-regulated dc power supply. The collecting electrode was connected through either of two integrating circuits to a Tektronix 7834 Storage Oscilloscope utilizing a 7A15A Plug-in with 500 μV/cm sensitivity and a 10 MHz bandwidth. To avoid space charge distortion of

the applied electric field, it was necessary to limit the electron pulses in these experiments to approximately 10^6 charges. The integration of the electron component of this small signal was performed on the 80 pf net capacitance of a short length of RG58 coaxial cable and the input capacitance of the scope plug-in. Typical electron transit times were several microseconds during which time a signal of several millivolts was developed on this integrator.

The 80 μsec RC time constant of the fast integrator made it unsuitable for observation of the ion component of the swarm signal which had a characteristic time scale of 100 μsec. However, the overall behavior of the swarm waveform was readily handled using an operational amplifier based integrator with a feedback capacitor of 50 pf and a time constant of tens of milliseconds. Thus, electron transit times were determined from the fast integrator signal and the relative contributions of electron and ion components were obtained using the second integrator circuit.

Photon Sources

During the course of the swarm studies, photoelectron emission was initiated by two alternate sources of illumination: a flash lamp pumped dye laser or a UV flashtube. A Phase-R Model DL-2100C dye laser was tuned by intracavity prisms to provide a polarized, 0.7 nm linewidth at 450 nm using Coumarin 450 dye in methanol. Irradiation of metal surfaces with the 300 nsec, 100 mJ pulses from this laser resulted in a satisfactory level of electron production by a nonlinear photoemission process[24], both in air and under vacuum conditions. However, it was discovered that this laser source was unsuitable for use in the $HgBr_2$ measurements for reasons to be discussed subsequently. The other photon source used in these studies was an EG&G FX-265 bulb-type xenon flashtube. Use of a 0.05 pf low inductance capacitor in the manufacturer's recommended circuit resulted in photoflashes of approximately 500 nsec duration and of sufficient UV yield to provide the 10^6 photoelectrons required experimentally. Single-shot data was acquired photographically from the oscilloscope which provided a delayed trigger to the flashtube and stored the resulting integrated current waveform.

C. Analysis of Swarm Experiments

Modeling

The pulsed swarm experiment is idealized by considering the electrons to move as a sheet between two electrodes under the influence of an applied electric field. At pressures where gas collisions dominate and when the electron concentration is sufficiently low to avoid space charge effects, the electron drift velocity and the electron energy distribution are characterized by the gas mixture and the prevailing electric field to gas density ratio, E/N. When attachers are present in a sufficient concentration in the gas mixture and when the applied E/N insures the presence of electrons at energies above the threshold for attachment, conversion of electrons to negative ions will take place[23]. Under these conditions, an exponential attenuation of the number of electrons in the sheet will occur as it sweeps across the gap. Left behind will be a spatially distributed group of negative ions which also slowly drifts toward the collector. The current induced in the external circuit as a result of the motion of these changes consists of an initial several microsecond electron spike superimposed on a slowly declining, low current component due to the less mobile negative ions. Integration of this induced current waveform has two practical benefits. First, it converts the fast, low-level current pulse into an experimentally observable voltage waveform and secondly, it makes the extraction of the attachment rate data especially straightforward.

A typical integrated waveform is displayed in Fig. 7a. The leading edge of a similar waveform is shown in Fig. 7b on an expanded time scale. Note that the initial rapid rise of the integrated current to a voltage level $V(t_e)$ ends at the electron transit time, t_e. This time corresponds to electrode separation, L, divided by the electron drift velocity, v_{de}, i.e.:

$$t_e = L/v_{de} \ . \tag{2}$$

A further slow increase in voltage follows until the last negative ions reach the collector from their origin near the emitter. At this time, which corresponds to the electrode separation, L, divided by the negative ion drift velocity, v_{dn},

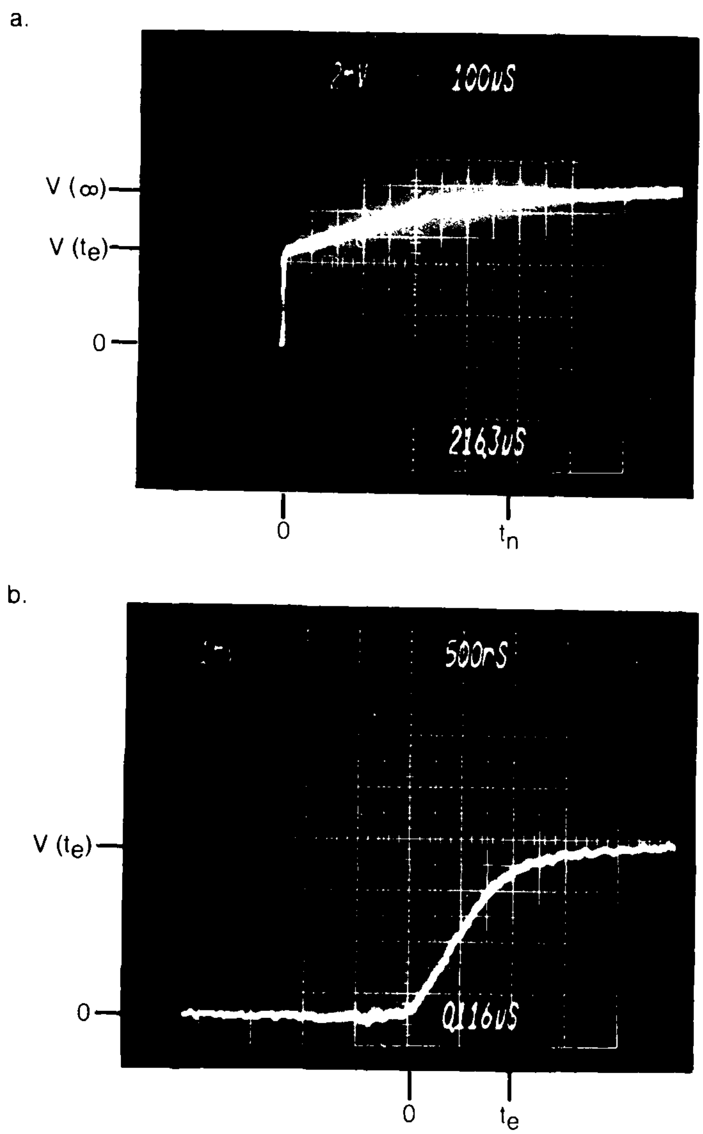

Figure 7. Integrated current waveforms from the pulsed, electron swarm experiment as displayed on two time bases: (a) 100 μsec/div, (b) 500 nsec/div. The full trace (a) exhibits a voltage jump due to electron motion followed by a prolonged rise to saturation as the ions drift from the interelectrode region. The signal from the fast integrator shows that the electron transit time is approximately 1 μsec for these conditions.

80-7-94 6

i.e.,

$$t_n = L/v_{dn} , \tag{3}$$

the current integral has attained its saturated value, $V(\infty)$. Mathematical modeling of the electron and negative ion currents and evaluation of their integrals reveals that the attachment rate coefficient, k_a, the concentration of the attaching gas, N_a, and the electron transit time, t_e, are related to observed voltages $V(t_e)$ and $V(\infty)$ by the expression[23]:

$$\frac{V(t_e)}{V(\infty)} = \frac{1-e^{-k_a N_a t_e}}{k_a N_a t_e} \tag{4}$$

Thus, measurement of the two voltages and the value of t_e, along with a knowledge of N_a permits computation of k_a, the attachment rate coefficient. A more complex expression[23] for this voltage ratio applies when volume ionization augments the number of electrons in the swarm. However, in the limit where ionization greatly exceeds attachment, the shape of the integrated current is similar to that associated with attachment and:

$$\frac{V(t_e)}{V(\infty)} = \frac{1-e^{-k_i N t_e}}{k_i N t_e} \tag{5}$$

where k_i is the mixture weighted ionization rate coefficient and N is the gas concentration. Experimentally, the onset of ionization is readily distinguished owing to the rapid increase in the saturation level, $V(\infty)$, with increasing E/N; thus, complications due to this effect can be avoided if desired. In addition, since it is often possible to utilize a mixture of attacher and buffer gas such that electron distribution function is controlled entirely by the buffer gas for which the cross sections are well known[9] (e.g., N_2 and rare gases), the measured electron drift velocity can be verified by comparison with a value determined from a Boltzmann analysis[25]. Thus, the measurement of the attachment rate coefficient as a function of E/N provides sufficient information to extract the attachment cross section itself. UTRC has unique capabilities as regards numerical analysis of swarm data, with the result that a wide variety of mixtures and experimental conditions could be examined and interpreted.

$N_2/HgBr_2$ Mixtures - Laser Source

Initial swarm studies were conducted in 0.1 atmosphere $N_2/HgBr_2$ mixtures using the dye laser to initiate the photoemission process. Nitrogen is a particularly good buffer in most measurements of this type because its very large cross sections dominate electron collisions and thereby control the electron transport properties and the electron energy distribution in the mixture. A characteristic waveform indicative of attachment was observed for a range of E/N values between 3Td and 70Td (1 Townsend = 1Td = 10^{-17} V-cm^2) in a gas mixture of 780 ppm $HgBr_2$ in N_2 at 1.8×10^{18} cm^{-3}. Analysis of these data implied attachment rate coefficients which increased with increasing E/N and had a magnitude in the 10^{-9} cm^3-sec^{-1} range. These findings were in very good agreement with preliminary, unpublished results of Nygaard and coworkers[7], who used a laser source and a similar $N_2/HgBr_2$ gas mixture. However, subsequent experiments at conditions of 450 ppm $HgBr_2$ in N_2 at a density of 1.4×10^{18} cm^{-3} revealed that the rate coefficients being extracted from the data did not exhibit the required independence to attacher concentration, a circumstance which prompted critical reevaluation of the experimental procedure. Detailed examination revealed that virtually all of the data for both $N_2/HgBr_2$ mixtures over the full span of E/N variation reduced to a constant $V(t_e)/V(\infty)$ ratio within a scatter of $\pm$ 10 percent. Thus, the inferred E/N behavior of rate coefficient was actually due primarily to the dependence of the electron drift velocity on E/N. The following experimental observations obtained using the laser to initiate photoelectrons indicated that the high rate coefficients inferred from these measurements and the inconsistent dependence on attacher concentration were experimental artifacts associated with the use of the high intensity laser pulse for photoelectric emission. The integrated current signals obtained with the emitter power supply at a negative potential implied both electron and negative ion components of the current as typified by the waveform of Fig. 7a. Application of a positive voltage to the emitter gave rise to a somewhat similar waveform of opposite polarity but with no initial jump in voltage which would signify electron motion. The absence of the electron component verified that this signal was not due to electron emission caused

by scattered light falling on the opposite electrode surface. Hence, the observed signal was due to motion of positive ions toward the collector. A consistent explanation for these experimental observations was that the high instantaneous intensity of the laser radiation even when defocused was sufficient to vaporize and ionize some of residual $HgBr_2$ on the electrode surface. From the resulting plasma either electrons and negative ions or positive ions could be extracted depending on the polarity of the applied voltage. Close examination of the electron/negative ion waveforms revealed a nearly linear rise to saturation in the portion of the waveform associated with the negative ion current. This linearity was consistent with the behavior expected when the negative ions were born at the emitter surface rather than throughout the volume. Additional supportive evidence for a laser source related explanation of these experimental observations is provided by the comparison of results obtained with the UV flashtube source as will be discussed subsequently. On the basis of these findings it was concluded that the preliminary $HgBr_2$ attachment rate coefficients originally reported by Nygaard and coworkers[7] and reproduced in these measurements are incorrect.

$N_2/HgBr_2$ Mixtures - UV Flashtube Source

Since the method described above provided no information regarding the volume electron attachment rate, the dye laser photosource was abandoned and all subsequent swarm studies utilized a UV flashtube. The $HgBr_2/N_2$ measurements were repeated under the same conditions as described above with photoelectrons provided by the flashtube system. No evidence of attachment was observed, suggesting a small rate coefficient. Therefore, the $HgBr_2$ concentration was increased to one part in 52 of N_2 at a 1.9×10^{18} cm^{-3} density. Waveforms similar to those in Fig. 7 were detected then at E/N values above 60 Td; however, the level of $V(\infty)$ also rose rapidly with increasing applied electric field signifying that ionization was being observed. Subsequent model calculations using the preliminary $HgBr_2$ ionization and attachment cross sections, which had become available at this time from the electron beam experiment, provided experimental guidance at this point. These computations[26] showed that in a N_2 buffer the direct ionization of $HgBr_2$ exceeds the loss of

electrons by attachment at all values of E/N where the attachment rate was sizeable enough to be measured accurately in the swarm experiment. This was shown to result from a rather fortuitous combination of factors: (1) the relative magnitudes of the attachment and ionization cross sections in $HgBr_2$; and (2) the location of the energy threshold for $HgBr_2$ attachment near 3 eV, a region characterized by an absence of electrons at low E/N's in N_2 due to the barrier at 2.0 eV provided by the resonance in the N_2 vibrational cross sections[25]. Thus, N_2 which is generally the buffer of choice in experiments of this type is uniquely ill-suited for the present purpose. Further analysis suggested that xenon would be a suitable buffer for these studies since the difficulties with the relative rates of attachment and ionization were peculiar to N_2.

Xe/$HgBr_2$ Mixtures

Use of Xe in place of N_2 in the buffer gas for $HgBr_2$ does introduce certain other differences. The E/N required to sustain an average electron energy of several electron volts is considerably lower in xenon than in N_2. At these reduced electric fields, the electron drift velocity is in the mid- 10^5 cm-sec^{-1} range. Consequently, the several microsecond electron transit time is now long compared to the 500 nsec duration of the UV flashtube pulse such that t_e can be measured accurately. It was not critical that the several hundred nanosecond transit times be measured in the nitrogen mixture since its large cross sections insured that electron-N_2 collisions would dominate electron transport. However, although Xe cross sections are well known[9], computed drift velocities are far less accurate since in this gas even very low levels of gaseous impurities or $HgBr_2$ itself will introduce low energy collision processes which modify the average electron energy and drift velocity dependence on E/N. This factor can significantly complicate the interpretation of the measured E/N dependence of the attachment coefficient but not appreciably alter the magnitude of the rate coefficient.

D. $HgBr_2$ Attachment Rate Coefficients

Pulsed electron swarm measurements of the $HgBr_2$ attachment rate coefficient were conducted in a Xe buffer with fractional mercuric bromide concentrations in the part per thousand range. However, at very low E/N values in this mixture it was not possible to conduct attachment measurements in the absence of a low level of an unidentified impurity which was associated with the introduction of $HgBr_2$ to the system. At low electron energies this impurity caused the experimentally determined drift velocities to exceed by a factor of two those computed[27] for the rare gas - $HgBr_2$ mixtures. In spite of repeated vacuum distillations of the $HgBr_2$ and frequent purges of the cell with buffer gas, the impurity persisted. However, at E/N values of greater than 7 Td the measured v_{de} was fractionally higher but otherwise in general accord with the E/N dependence computed for the Xe/$HgBr_2$ mixture. Therefore, attachment measurements proceeded with the recognition that assignment of an average electron energy to data obtained especially at certain low E/N values would require additional information.

Shown in Fig. 8 are the attachment coefficients obtained from swarm measurements in a Xe buffer. Also plotted are computed values of k_a obtained using the previously described beam-measured cross section for attachment. The ionization rate coefficients for Xe[9] and $HgBr_2$ are also indicated. On this figure, the xenon ionization rate coefficient has been multiplied by 1000 to reflect its relative mixture weighted importance in the ionization process and to permit direct comparisons with the experimental results.

Focusing first on the computed results, note that although $k_i(HgBr_2)$ exceeds $k_i(X_e)$ by at least a factor of ten, ionization of xenon will dominate in the nominal 1000:1, Xe/$HgBr_2$ mixtures used in these studies. However, as E/N is reduced, ionization decreases very rapidly and attachment dominates electron kinetics. Further reduction of E/N ultimately reduces to a small fraction the number of electrons in the distribution with energies above the 3.1 eV threshold for attachment and k_a then falls precipitously.

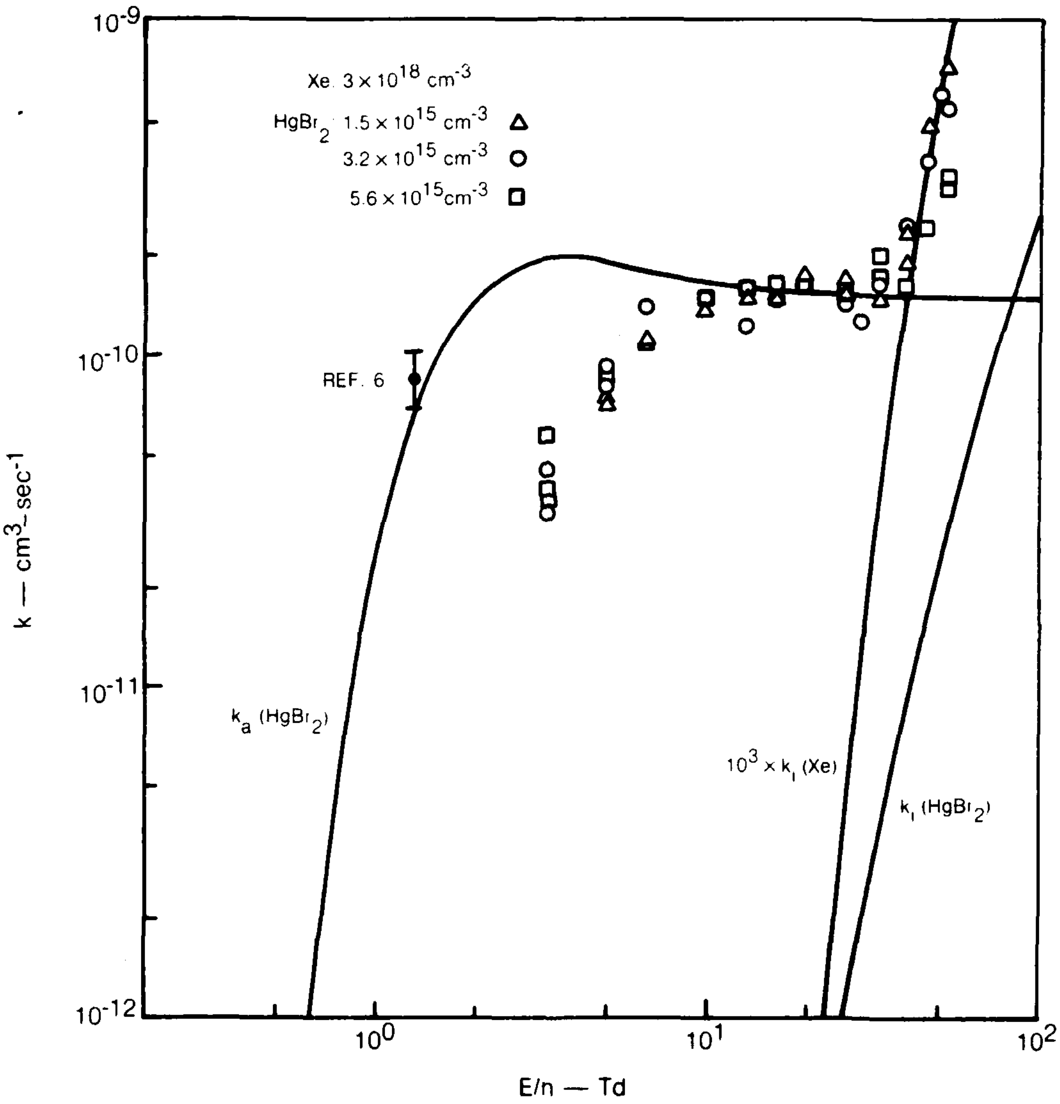

Figure 8. Comparison of rate coefficients obtained by the swarm method with those computed from the measured $HgBr_2$ cross sections. The k_i(Xe) values have been multiplied x 10^3 to facilitate direct comparison with the data (●). The single point at 1.3 Td is the data of Degani, Rokni and Yatsiv (Ref. 6).

80-7-94-7

The experimental results for Xe buffered mixture at three concentrations of $HgBr_2$ are also shown in Fig. 8. These values of k_a and k_i were obtained from Eqs. 4 and 5 using the measured voltage ratios, $V(t_e)/V(\infty)$, and the observed electron transit times. At the highest E/N values, a rapid growth of the measured rate was determined. Comparison with the computation clearly indicates that this component of the measured rate coefficient is due to xenon ionization. At somewhat lower E/N values between 10 Td and 30 Td ($\sim$ 4 eV average electron energy) the measured, nearly constant rate coefficient of 1.5×10^{-10} cm^3-sec^{-1} is in very good agreement with the computed value for Br^- formation. However, further reduction of the electric field causes an observed decline in the inferred k_a at E/N values greater than those computed for the $Xe/HgBr_2$ mixture. This behavior is anticipated since the effect of an impurity at low E/N is a premature cooling of the electrons (i.e., lowering of the energy of the electron distribution) to a value below that which would prevail in the pure mixture. Except at the E/N values below 10 Td where the assignment of an average electron energy is in doubt, the predictable electron drift velocity behavior and the good agreement between the swarm-measured rate and the comparable rate derived from the measured attachment cross section serves to verify the results of these independent measurements methods.

Also shown in Fig. 8 is a single data point which represents a determination of the $HgBr_2$ attachment rate coefficient by Degani, Rokni and Yatsiv[6]. This data was obtained by observing the rate of decay of the electron density in a $Xe/HgBr_2$ mixture following flash X-ray ionization. The measured value of 8.5×10^{-11} cm^3-sec^{-1} is found to be in very good agreement with the computed rate coefficient based on attachment cross section determined in the present investigation, a circumstance lending considerable support to the interpretations discussed in the previous paragraphs. The suggestion of Rokni and coworkers[6] that the reaction $e + HgBr_2 \rightarrow Br^- + HgBr$ actually produces HgBr in the B-state is consistent with the present observation that the threshold for attachment in $HgBr_2$ occurs at 3.1 eV although essentially zero energy attachment is energetically possible.

E. $HgBr_2$ Ionization Rate Coefficients

A measurement of the mercuric bromide ionization rate coefficient over a range of E/N values was obtained in swarm studies using N_2 as the buffer gas. For the reasons cited above, ionization of $HgBr_2$ dominates attachment in N_2 mixtures. This circumstance has provided an unanticipated verification of the beam-measured ionization cross section.

Electron distribution function calculations of the rate coefficients for ionization and attachment in a $N_2/HgBr_2$ (0.98/0.02) mixture were performed using the $HgBr_2$ ionization and attachment cross sections determined in the electron beam measurements. The computed dependencies of $k_a(HgBr_2)$, $k_i(HgBr_2)$ and $k_i(N_2)$ on E/N are shown as solid lines in Fig. 9 for a span of that parameter from 40 Td to 240 Td. This range of E/N corresponds to average electron energies in the 1.1 eV to 6.0 eV range of interest in laser discharge analysis. Also shown for the same gas mixture are data points obtained from laboratory measurements of the integrated current waveforms using Eq. 5. Note that even at its 50 to 1 preponderance over $HgBr_2$, the N_2 makes only a small contribution to the total ionization rate and that except at the lower E/N values, $HgBr_2$ attachment is small relative to its ionization rate. Analysis of this lower electron energy data taking into account simultaneous electron production and loss[23] indicates that the data point at E/N = 65 Td, where $k_i \simeq k_a$, should be reduced by a factor of two to reflect only the ionization contribution. This is indicated by the arrow in Fig. 9. The other data points require proportionately smaller downward adjustments.

The generally good agreement between the mercuric bromide ionization rate coefficient obtained by the swarm method and its counterpart computed from the measured total cross section for the same process provides strong support for the values obtained from both methods. The swarm results are especially pertinent to discharge modeling since it is in the threshold region that the ionization cross section weights most heavily both in pulsed swarm studies and in fast pulse laser discharge operation.

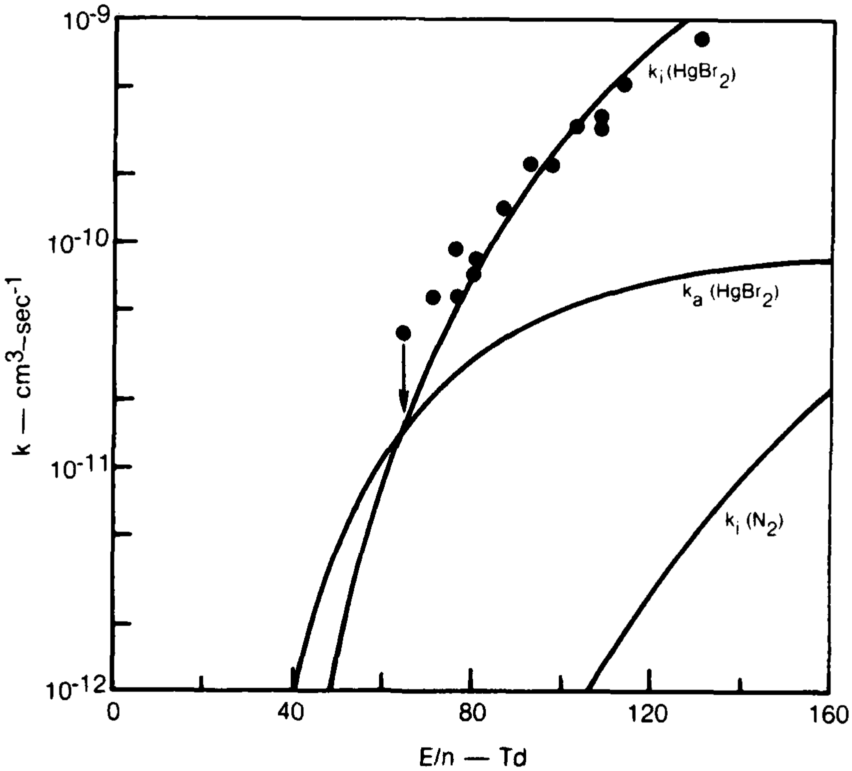

Figure 9. Rate coefficients for electron attachment and ionization in a N_2/HgBr (0.98/0.02) mixture. The mercuric bromide results are based on the cross sections measured in this work.

80-7-94-8

IV. DISCUSSION

Under this program the electron impact ionization and attachment cross sections for $HgBr_2$ and the corresponding rate coefficients for these processes have been measured. Details of these investigations have been described in Sections II and III. In this section, the experimental results will be related to published information on $HgBr_2$ and the implications of these findings to the charged particle kinetics of the mercuric bromide laser will be discussed.

A. Positive Ion Kinetics

Only one previous mass spectrometric survey of positive ion formation in $HgBr_2$ has been reported[19,20]. However, accurate threshold energies for photoionization to various ion states of $HgBr_2^+$ are available[28]. In addition, bond energies associated with $HgBr_2$ and HgBr are listed in the thermochemical literature[29]. The ionization potentials, appearance potentials and thermochemical thresholds for products of electron-$HgBr_2$ collisions obtained from these sources are summarized in Table I. Also indicated are the corresponding results of the present investigations.

TABLE I

IONIZATION POTENTIALS, APPEARANCE POTENTIALS, AND THERMOCHEMICAL THRESHOLDS FOR PRODUCTS OF ELECTRON-$HgBr_2$ COLLISIONS

	Literature (eV)	This Work (eV)
$HgBr_2^+$	9.94[a], 10.62[b]	10.6 ± 0.1
$HgBr^+$	12.09[a]	12.2 ± 0.2
Br^+	16.7[a]	17.2 ± 0.3
Hg^+	14.2[c]	15.5 ± 0.2
Br^-	~3 @ PEAK[a]	3.1; 3.7 @ PEAK
Br·HgBr	3.07[d]	
Hg·Br	0.75[d]	

a. Refs. 19, 20 b. Ref. 28 c. Ref. 30 d. Ref. 29

Comparison of the appearance potentials obtained in this work with those obtained by Kiser, Dillard, and Dugger[19], indicates qualitative agreement. However, the ionization potential (IP) of the parent molecule measured in the present study, 10.6 eV, is in better agreement with the more accurate determination of 10.62 eV obtained from the photoelectron spectra of $HgBr_2$[28]. Further, an important feature of both mass spectrometer measurements is the appearance potential of the $HgBr^+$ ion at slightly above 12 eV. From this threshold and the Br·HgBr bond energy of 3.07 eV, an ionization potential of 9.1 eV or less is inferred for HgBr. Since this value is below IP($HgBr_2$), charge exchange from $HgBr_2^+$ or from many other potentially available ions to HgBr is energetically possible. Moreover, since such ions frequently form clusters in high pressure gas backgrounds, it is not surprising that $HgBr_2^+$ and $Hg_2Br_3^+$ ($HgBr^+ \cdot HgBr_2$) ions were recently observed at high N_2 pressures in a drift tube experiment[31].

Mercuric bromide lasers have been operated at approximately atmospheric pressures in both $Ne/N_2/HgBr_2$ or $Ne/Xe/HgBr_2$ mixtures. In these laser mixtures the $HgBr_2$ vapor represents a few tenths of a percent of the total gas content and the N_2 or Xe constitute nominally 10 percent. In the fast-pulsed, self-sustained laser discharges, all of which utilize the N_2 mixture, the large ionization cross section of $HgBr_2$ and its low ionization potential insures that $HgBr_2^+$ formation will represent a significant fraction of the total ion production. Little conversion to $HgBr^+$ or cluster ions is expected due to the 100 nsec discharge duration and the limited accumulation of HgBr during this short pulse. However, the situation in electron beam sustained discharges is different for several reasons. In these lasers, the energetic electrons form the parent ion species approximately in proportion to the composition of the laser mixture. Thus, the combinations, Ne^+/N_2^+ or Ne^+/Xe^+, will constitute the bulk of the positive ions initially. However, through a series of ion kinetic reactions involving clustering and charge exchange[31], these will be converted to $HgBr_2^+$ on a 100 nsec time scale. Since e-beam laser pulses can approach 1 μsec durations, accumulation of a significant HgBr content by way of the laser transition is probable. Under these conditions substantial conversion to $HgBr^+$ or

cluster ions is likely. These ion conversions will only matter to mercuric bromide laser performance if these intermediate or ultimate ion species exhibit significantly different electron-ion/ion-ion recombination rates or photoabsorption characteristics at 502 nm. Little detailed information concerning these aspects of the positive kinetics is currently available for mercuric bromide dissociation lasers.

B. Negative Ion Kinetics

Little previous data are available on negative ion formation from $HgBr_2$ as indicated also in Table I. Kiser, Dillard and Dugger[19,20] found only Br^- formation at ∿ 3 eV in their mass spectrometer studies. These investigators noted that no negative ions were formed in ion pair processes. The present experimental results are generally in agreement with these earlier observations, except that both the attachment process and the ionization of the parent molecule were found to occur at approximately 0.7 eV higher energies than previously noted. This is the extent of current knowledge on negative ion formation from $HgBr_2$; however, slightly more data is available on its chlorine analog, $HgCl_2$. This data may be useful in suggesting possible ion types to be expected in high pressure situations, since in their mass spectrometer studies, Kiser, et al.[19], observed that generally the negative ion processes in the $HgBr_2$ and $HgCl_2$ were analogous. At somewhat higher ionization chamber pressures in a mass spectrometer, Cohen[32], found not only $HgCl_2^-$ but $HgCl^-$ and $HgCl_3^-$ ($HgCl_2 \cdot Cl^-$) which he considered to be due to ion-molecule reactions. By analogy, these observations suggest that both $HgBr_2^-$ and $HgBr^-$ can be stabilized by third-body collisions and that $HgBr_2 \cdot Br^-$ or a similar cluster ion will quite likely exist at the high background pressures typical of laser operation.

The nature of the electron production process in fast-pulse lasers requires that the total ionization rate exceed the loss rate due to attachment at least during the early stage of the discharge. The initiation of the discharge occurs at high E/N values, such as to satisfy this requirement which is facilitated in the case $HgBr_2$ by its comparatively low attachment rate. During the discharge the negative ion-positive ion recombination process works in parallel with the electron-ion loss to limit the charge particle density but is not a critical factor in

discharge behavior. Even the contribution of $HgBr_2^+ - Br^-$ recombination to the HgBr B-state production is overwhelmed by the N_2 A-state transfer mechanism[3]. As with the positive ions, the 100 nsec characteristic time scale of the transient should limit conversion to clustered negative ions. In the electron-beam sustained discharges, the ionization provided by the source is balanced by the electron loss due to attachment. Analysis of current and voltage waveforms obtained under Navy contract[5] in the UTRC electron-beam laser facility using the Ne/Xe/$HgBr_2$ mixture provides an estimate of the attachment rate coefficient. A value of approximately 1×10^{-10} cm^3-sec^{-1} obtained from these data is in good agreement with the value measured in this program. The comparatively low attachment rate of $HgBr_2$ permits somewhat higher electron densities to prevail than would be the case for a similar source intensity in most other excimer lasers containing halogen molecules. Moreover, the lengthened time scale and high pressure of this type of laser and the expected accumulation of HgBr during the discharge suggest that ions such as $HgBr_2^-$, $HgBr^-$, and $HgBr_2{\cdot}Br^-$ may be prevalent during the latter protions of the pulse. Again, as with the positive ions, the significant of these ion conversions to laser performance depends on their comparative rates of ion-ion recombination or whether any absorb at the laser wavelength. No information is currently available regarding these matters.

V. SUMMARY AND RECOMMENDATIONS

A. Principal Results

Basic data on mercuric bromide electron attachment and ionization kinetics have been obtained. Total and partial cross sections for these reactions have been measured in an electron beam experiment and corresponding rate coefficients have been determined independently in a pulsed electron swarm apparatus. A number of important findings have resulting from these investigations:

- The ionization cross section of $HgBr_2$ increases from threshold at 10.6 eV to a value of 2×10^{-15} cm^2 at 70 eV.
- $HgBr_2^+$ is the principal positive ion product.
- The dissociative attachment cross section of $HgBr_2$ has a 3.1 eV threshold, a peak value of 1×10^{-17} cm^2 at 3.7 eV and an energy width of 1.4 eV.
- Br^- and possibly $HgBr_2(B^2\Sigma^+)$ are the products of the electron dissociative attachment reaction.
- The $HgBr_2$ attachment rate coefficient in the range of average electron energies of interest in laser applications is 1.5×10^{-10} cm^3-sec^{-1}, a value found to be relatively insensitive to gas mixture and/or E/N. For a specific mixture the attachment rate coefficient computed using a Boltzmann analysis and the cross sections determined from this investigation is estimated to have an accuracy of $\pm$ 30 percent.
- The attachment rate coefficient obtained from this investigation is in good agreement with a value obtained recently from studies of flash X-ray ionized $Xe/HgBr_2$ mixtures and is also consistent with the results of UTRC e-beam controlled discharge experiments and with modeling of mercuric bromide laser discharge characteristics.

B. Recommendations for Additional Work

This program has revealed a number of aspects of the kinetic processes in mercuric bromide dissociation lasers which require further investigation. The following discussion illustrates several particularly important factors, the investigations of which are compatible with the existing UTRC facilities.

- It is probable that the second product of the $Br^-/HgBr_2$ dissociative attachment reaction is the upper laser level, $HgBr(B^2\Sigma^+)$. While formation of the B-state by this process does not significantly effect the laser emission, its apparent predominance does raise the question of why the corresponding attachment process which results in HgBr ground-state production is not observed. Since the energetics of the reaction leading to ground-state $HgBr(X^2\Sigma^+)$ permits nearly zero energy attachment, the absence of any evidence for this process in the present investigation, in which the $HgBr_2$ is not excited vibrationally, suggests the possibility of a strong vibrational temperature dependence of the $Br^-/HgBr_2$ process in the vibrationally active laser environment. For this reason, positive identification of the neutral product of the presently observed dissociative attachment reaction should be made and experimental evidence for a vibrational temperature dependence of $HgBr_2$ attachment should be sought.

- A second feature which can influence the ion kinetics of $HgBr_2$ dissociation lasers is the appreciable production (> 10%) of HgBr which results from the laser action itself. The attachment characteristics of the Br and HgBr fragments due to electron impact and 3-body collisions in high pressure gas backgrounds should be examined. Since the potential curve for $HgBr^-$ is likely to cross that of HgBr in the vicinity of the equilibrium internuclear separation of the latter, zero electron energy attachment exhibiting a strong HgBr vibrational temperature dependence is probable. Since $HgBr_2$ may not exhibit low energy attachment even when vibrationally excited, even small quantities ($\sim$ 10%) of HgBr could contribute disproportionately to the loss of electrons by attachment. Unfortunately, essentially no kinetic data on HgBr is available.

• The instability thresholds and the discharge impedances of excimer lasers can be favorably influenced by modifying the attachment loss rate. Since the $HgBr_2$ attachment rate coefficient is comparatively low, the use of a second, chemically compatible attacher with $HgBr_2$ to raise the attachment rate may prove beneficial to discharge performance. For example, the net electron attachment rate in $HgBr_2$ mixtures containing small amounts of a strong attacher such as HCl should be investigated. Thermochemical analysis at UTRC has already demonstrated that such chlorine and bromine compounds are chemically compatible.

• Laser experiments have shown that at $HgBr_2$ fractional concentrations near 1 percent are about optimum. At this relatively high level in a Ne/Xe laser mixture electron energy loss due to vibrational and electronic excitation of $HgBr_2$ is likely to be significant. The $HgBr_2$ electron energy exchange collision frequency can be determined by observing the $HgBr_2$ concentration at which the drift velocity in pure rare gas mixtures first begins to change. Boltzmann analysis can then be used to interpret the $HgBr_2$ cross sections required to result in this change of the measured drift velocity of the mixture. This technique is particularly well-suited to the existing UTRC drift/swarm experiments and would provide valuable additional information on electron-$HgBr_2$ collision processes and possibly e-HgBr reactions as well.

Laser modeling and experimentation has served to identify the need for improvements in the HgBr/$HgBr_2$ data base suggested above. The facilities and experience gained in connection with the present program uniquely qualifies UTRC to carry out this additional research.

REFERENCES

1. Schimitschek, E. J. and J. E. Celto: Appl. Phys. Lett. 36, 176 (1980).
2. Brown, R. T. and W. L. Nighan: Appl. Phys. Lett. (in press).
3. Chang, R. S. F. and R. Burnham: Appl. Phys. Lett. 36, 397 (1978).
4. Dreiling, T. D. and D. W. Setser: Chem. Phys. Lett. (in press).
5. Contract N00014-78-C-0830. The work is reported in Ref. 2. The inferred rate coefficient for electron attachment was $k_a \cong 1 \times 10^{-10}$ cm^3-sec^{-1} for the laser mixture.
6. Degani, J., M. Rokni, and S. Yatsiv: J. Chem. Phys. (in press).
7. Brooks, H. L., R. A. Sierra, K. J. Nygaard and J. A. Fletcher: (unpublished).
8. Tate, J. T. and P. T. Smith: Phys. Rev. 39, 270 (1932).
9. Rapp, D. and P. Englander-Golden: J. Chem. Phys. 43, 1464 (1965).
10. Briglia, D. D. and D. Rapp: J. Chem. Phys. 42, 3201 (1965).
11. Rapp, D. and D. D. Briglia: J. Chem. Phys. 43, 1480 (1965).
12. Chantry, P. J.: Phys. Rev. 172, 125 (1968).
13. Kurepa, M. V. and D. S. Belic: J. Phys. B 11, 3719 (1978).
14. Kurepa, M. V., V. M. Pejcev and I. M. Cadez: J. Phys. D 9, 481 (1976).
15. Vapor pressures for $HgBr_2$ were computed from the JANAF thermochemical tables (Stull, D. R. and H. Prophet: Nat. Stand. Ref. Data Ser. 37, (1971)) for the range of temperatures 300°K to 600°K. Pressure at 300°K is 1.2×10^{-4} torr and at higher temperatures is consistent with the tabular data listed by L. Brewer in: The Chemistry and Metallurgy of Miscellaneous Materials, Edited by L. L. Quill (McGraw-Hill, New York, 1950).
16. Fox, R. E., W. M. Hickam, D. J. Grove and T. Kjeldaas: Rev. Sci. Instrum. 26, 1101 (1955).
17. Chantry, P. J.: Rev. Sci. Instrum. 40, 884 (1969).
18. Rosenstock, H. M., K. Draxl, B. W. Steiner and J. T. Herron: J. Phys. Chem. Ref. Data 6, Suppl. 1, (1977).
19. Kiser, R. W., J. G. Dillard and D. L. Dugger: Advan. Chem. Ser. 72, 153, (1968).

REFERENCES (Cont'd)

20. Dillard, J. G.: Chem. Rev. 73, 589 (1973).

21. The relative abundance of the product ions at 70 eV are: $HgBr_2^+$ (100.0), $HgBr^+$ (17.5), Br^+ (34.3), Hg^+ ($\sim$ 0) as listed in Ref. 19.

22. Grünberg, R.: Z. Naturforsch. 24a, 1039 (1969).

23. Nygaard, K. J., H. L. Brooks and S. R. Hunter: IEEE J. Quantum Electron. QE-15, 1216 (1979).

24. Anisimov, S. I., V. A. Benderskii and G. Farkas: Sov. Phys. USP. 20, 467 (1977).

25. Nighan, W. L.: Phys. Rev. A 2, 1989 (1970).

26. Final computations using the beam-measured cross sections for $HgBr_2$ and the well known N_2 values, Ref. 9, are shown in Fig. 9 and discussed further in its description.

27. The Boltzmann code computations for the electron drift velocities were performed using the methods of Ref. 25. Calculated drift velocities in the mixtures did not depart significantly from those of the pure gas.

28. Eland, J. H. D.: Int. J. Mass Spectrom. Ion Phys. 4, 37 (1970).

29. Vedeneyev, V. I., L. V. Gurvich, V. N. Kondrat'yev, V. A. Medvedev and Ye. L. Frankevich: Bond Energies, Ionization Potentials and Electron Affinities. St. Martin's Press, New York. 1966.

30. The sum of the energy required to dissociate $HgBr_2$ into its fragments and the ionization potential of Hg^+ (Ref. 29).

31. Johnsen, R. and M. A. Biondi: Bull. Am. Phys. Soc. 25, 108 (1980).

32. Cohen, S. C.: Inorg. Nucl. Chem. Letters 6, 757 (1970).

R80-924780-1

July 31, 1980

Distribution List

Scientific Officer Director, Physics Program Physical Sciences Division Office of Naval Research 800 North Quincy Street Arlington, Virginia 22217 Attn.: M. B. White - NR 395-594 Ref.: Contract N00014-79-C-0593	1 copy (with DD 250)
AF Plant Representative Office (OL-AA) Pratt & Whitney Aircraft Group East Hartford, CT 06108 Attn.: Mr. C. R. Paoletti	1 copy
Director, Naval Research Laboratory Attn.: Code 2627 Washington, D. C. 20375 DODAAD Code N00173	6 copies
Defense Documentation Center Bldg. 5, Cameron Station Alexandria, Virginia 22314 DODAAD Code S47031	12 copies
Office of Naval Research Branch Office - Boston 666 Summer Street Boston, Mass. 02210 DODAAD Code N62879	1 copy
Dr. E. J. Schimitschek Code 811 Naval Ocean Systems Center 271 Catalina Blvd. San Diego, CA 92152	1 copy

Distribution List (Cont'd)

Dr. Robert E. Behringer Office of Naval Research 1030 East Green Street Pasadena, California 91101	1 copy
Dr. R. Burnham Laser Physics Branch Naval Research Laboratory Washington, D. C. 20375	1 copy